Design, Fabrication and Analysis of a Mach-Zehnder Interferometer

Louisa Catharina Schneider
Senior Process Development Engineer
Louisa.Schneider@SkyWaterTechnology.com

SkyWater Technology Foundry
2401 E 86th St
Bloomington, MN 55425

DOI: 10.1109/JPHOT.2017.XXXXXXX
1943-0655/$25.00 ©2017 IEEE

Manuscript received July 25th, 2017; revised September 10, 2017.
The participation in the edX online class "Silicon Photonics Design, Fabrication and Data Analysis" was sponsored by SkyWater Technology Foundry.

Abstract: In this class project, Mach-Zehnder Interferometers (MZI) are designed and fabricated using a variety of different imbalance lengths. The difference in imbalance length of an MZI is investigated, as well as its effect on the free-spectral range (FSR). Simulations and numerical curve fitting methods are used to extract the waveguide (WG) properties (effective index, group index and dispersion) from the experimental data. The devices are fabricated on a SOI substrate and are designed to operate at a wavelength of 1550 nm.

Index Terms: Mach-Zehnder Interferometer (MZI), Silicon Photonics, Strip waveguides

1. Introduction

Silicon Photonic Circuits (PIC) contributed to the rise of optical communications due to its potential of combining the speed and compactness of photonics with the functionality and standardized fabrication techniques available for conventional CMOS devices [1]. In general, silicon photonic circuits can be separated in active (i.e. laser, to generate light) and passive (i.e. waveguides, waveguide bends, Y-branches, fiber grating couplers; used to rout the light across the circuit) components.

In this class project, a Mach-Zender Interferometer (MZI) is studied. A simplified representation of an MZI is shown in figure 1.

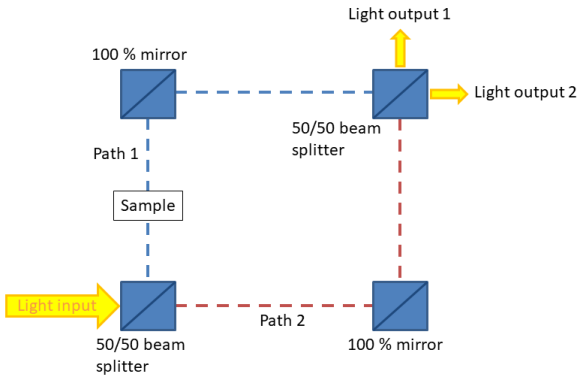

Fig. 1: Simplified schematic of a Mach-Zehnder Interferometer (MZI)

At the input, the light gets split and travels in equal parts in path 1 and path 2, where the sample inserted in path 1 introduces a phase shift. At the output, the light gets recombined and either constructive or destructive interference patterns can be observed, depending on the relative phase shifts between two optical paths. In the ideal case, a π-phase shift results in destructive interference (all light will be extinct), and an identical phase shift will result in constructive interference (maximum light intensity at the output). This property of the MZI enables its use as optical switch and basic building block for photonic logic, where the constructive and destructive interference can be thought of ”Ones” and ”Zeros” similar to the way it has been done in electrical integrated circuits for decades. The obvious advantage of using light for computation is that by using photons we can achieve a much higher bandwidth compared to using electrons for signal processing, which means photonic integrated circuits (PIC) can operate at much faster speeds while maintaining a low power consumption.

2. Theoretical Background

In order to implement the MZI as optical switch on a silicon wafer, the basic schematic can be thought of as shown in figure 2 (not shown are the grating couplers, which are needed to couple light in and out of the MZI). Y-branches are used as beam splitters, and WGs act as optical phase shifters.
The Mach-Zehnder Interferometer (MZI) can be constructed using three main elements: sub-wavelength grating couplers, Y-branches and waveguides. Y-branches can be used for two purposes: to split light from one waveguide equally into two waveguides or to combine light from two waveguides into one. A gds screenshot of a Y-branch used in this class is shown in figure 3. The insertion loss for this Y-branch splitter was found to be less than 0.3 dB [2].

2.1. Y-branch splitter

When used as splitter, the Y-branch splits the intensity of the light in two equal parts:

$$I_1 = I_2 = \frac{I_{in}}{2} \tag{1}$$

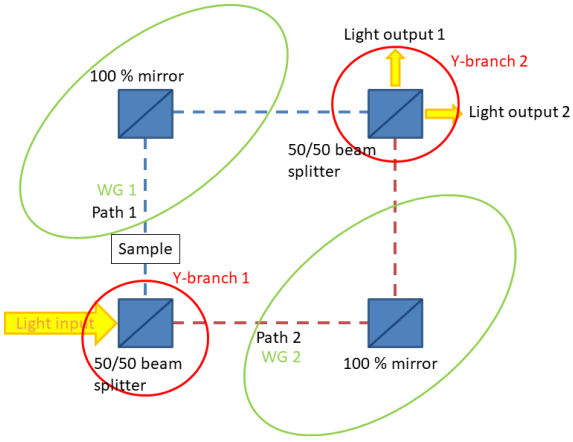

Fig. 2: Simplified schematic of an MZI used in a photonic circuit

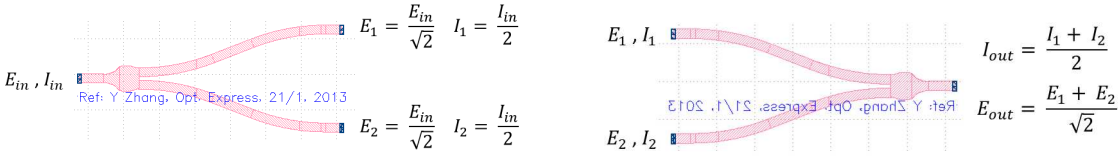

(a) Y-branch as splitter (b) Y-branch as combiner

Fig. 3: Example of a Y-branch [3]

since $I \propto |E|^2$, the electric field is given as

$$E_1 = E_2 = \frac{E_{in}}{\sqrt{2}} \tag{2}$$

2.2. Y-branch combiner

When light of two waveguides is combined, the intensity at the output of the Y-branch will be

$$I_{out} = \frac{1}{2} \cdot (I_1 + I_2) \tag{3}$$

and the electric field at the output is

$$E_{out} = \frac{1}{\sqrt{2}} \cdot (E_1 + E_2) \tag{4}$$

2.3. Waveguides

A **waveguide** (WG) is a structure used to guide light, where one (planar WG) or two (strip WG) spatial regions are restricted (light is confined). The WG core is made of material with a high refractive index (i.e. Si) surrounded by a material with lower refractive index (i.e. SiO_2, which is sometimes referred to as cladding oxide). This arrangement of low-high-low refractive indices enables total internal reflection, which is essential for the WG to confine and propagate light and prevents light from escaping into the cladding.

The time-depended electric field of a plane wave traveling in z-direction is given as

$$E = E_0 \cdot e^{j(\omega t - \beta z)} \tag{5}$$

using the complex **propagation constant** β

$$\beta = 2\pi \cdot \frac{n_{eff(\lambda)}}{\lambda} - i \cdot \frac{\alpha}{2} \tag{6}$$

and the radial frequency ω

$$\omega = 2\pi f = \frac{c}{\lambda} \tag{7}$$

The complex propagation constant β takes into account the effect of dispersion and loss (using the attenuation constant α) and determines how amplitude and phase vary along the propagation direction z [4].

The **refractive index** is the ratio of the speed of light in vacuum and the speed of light in a given bulk media for any given wavelength λ:

$$n(\lambda, T) = \frac{c}{v(\lambda, T)} \tag{8}$$

In general, the refractive index depends on λ and temperature, the values for silicon and silicon dioxide are given in table I. SiO_2 has a weak dependence and can be considered as constant.

	Si	SiO_2
Refractive Index	3.47	1.44
λ dependence: $\frac{dn}{d\lambda}$ $[nm^{-1}]$	$-7.6 \cdot 10^{-5}$	$-1.2 \cdot 10^{-5}$
Temperature dependence: $\frac{dn}{dT}$ $[K^{-1}]$	$1.87 \cdot 10^{-4}$	$8.5 \cdot 10^{-6}$

TABLE I: Refractive Index for Si and SiO_2 [5]

The **effective index** n_{eff} differs from the refractive index since it considers the light propagating in a guided structure (i.e. a waveguide, where x- and/or y-directions are confined) compared to an infinite bulk medium (i.e. no confinement in x/y/z direction). In more general terms, n_{eff} is a number that quantifies the phase velocity per unit length in a waveguide, relative to the phase velocity in vacuum. It depends on the wavelength λ and on the mode in which the light propagates (which in turn is also depending on the geometry of the waveguide) [6].

The **phase velocity** of the light traveling through a waveguide is given as

$$v_p(\lambda) = \frac{c}{n_{eff}} \tag{9}$$

The **group velocity** is

$$v_g(\lambda) = \frac{c}{n_g} \tag{10}$$

v_g can be understood as the velocity with which the overall shape of the wave (the envelope) propagates through space. The group velocity dispersion describes how a

pulse spreads in an optical fiber. Since the pulse is related to n_g, information always travels slower than the phase velocity v_p (which is related to n_{eff}.

The **group index** n_g is used to determine the **free-spectral range** (FSR), which can be visualized as the shift in effective index vs. wavelength (i.e. the spacing between adjacent peaks):

$$n_g(\lambda) = n_{eff}(\lambda) - \lambda \cdot \left(\frac{d}{d\lambda} n_{eff}(\lambda) \right) \tag{11}$$

The FSR for a MZI is given as [5]

$$FSR = \frac{\lambda^2}{\Delta L \cdot n_g(\lambda)} \tag{12}$$

The FSR depends on the imbalance length ΔL and the group index n_g of the WG.

In general, **dispersion** can be a combination of material dispersion and WG dispersion. Material dispersion describes the propagation dependence of optical wavelengths at different velocities on the refractive index of the material. Waveguide dispersion causes more light to leak into the cladding when traveling along the WG.

2.4. Grating couplers

A grating coupler is necessary to couple light from free space into the waveguide and vice versa. The grating coupler has been optimized and is part of the gds library used in this class. A gds screenshot is shown in figure 4a; figure 4b shows a SEM image of an actual fabricated GC.

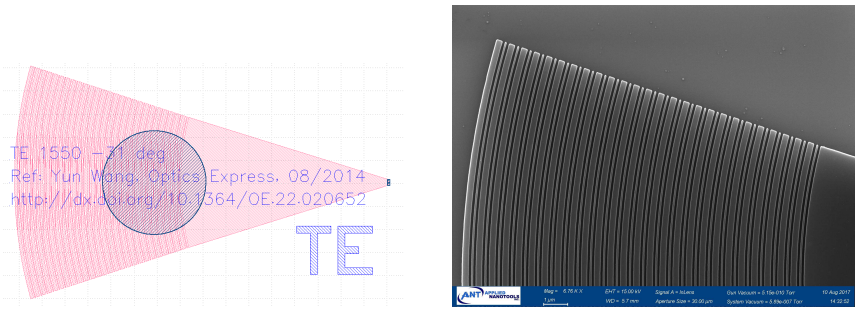

(a) gds design of a GC (b) SEM image of a GC (zoomed in)

Fig. 4: Example of a grating coupler (GC) [3]

Due to the optical testing setup used in this class at University of British Columbia, the vertical distance (pitch) is set to 127 μm, and all GC used for TE polarized light have to face to the left (GC for TM polarized light need to face to the right to avoid the need for rotating the chips for automated measurements).

2.5. Mach-Zehnder Interferometer

The transfer function for a loss-less, imbalanced (i.e. path length of both waveguides are not equal, $\Delta\lambda = L_1 - L_2$) interferometer is given as [7]

$$\frac{I_{out}}{I_{in}} = \frac{1}{2}\{1 + \cos(\beta \cdot \Delta L)\} \tag{13}$$

assuming $L_1 \neq L_2$ and $\beta_1 = \beta_2$. ΔL is the imbalance length of the MZI.

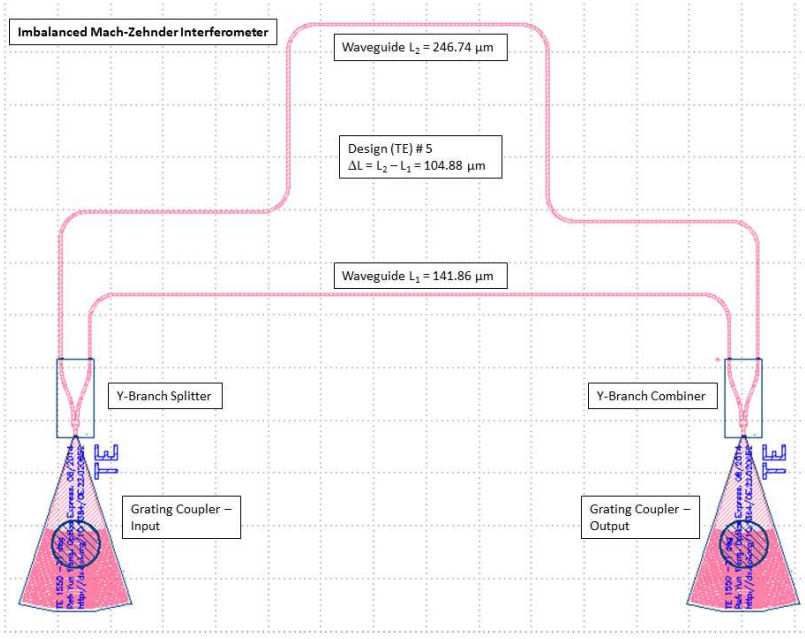

Fig. 5: gds layout of a Mach-Zender Interferometer with an imbalance length of 105 μm

An imbalance in length introduces an additional phase shift in one arm of the MZI and results in a periodic transfer function with respect to λ. This periodicity is what is defined as FSR (see equation 12). Figure 5 shows an example of an MZI with an imbalance length of 105 μm.
The output intensity (in dB) is given as

$$I_{out} = 10 \cdot \log_{10}\left(|E_{out}|^2\right) \tag{14}$$

The insertion loss (in dB) is defined as

$$IL = P_{in} - P_{max} \tag{15}$$

3. Modeling and Simulation

3.1. Design Parameters

The available space to be used for this project is $605\mu m \times 41\mu m$. The top Si thickness is fixed to be 220 nm and the waveguides are designed for a width of 0.5 μm. The center wavelength is 1550 nm, and only strip waveguides are used in this class. The advantage of using a strip WG is that it can be fabricated using a single etch only and it allows tight bends with low optical loss (2-3 dB/cm). Figure 6 shows the gds design, which includes

several TE-mode MZIs and two TM-mode MZIs. Design #4 (TE-mode) and #2 (TM-mode) are de-embedding structures (two fiber grating couplers connected with a 195 μm long waveguide) which are used to calibrate the measurement system's insertion loss.

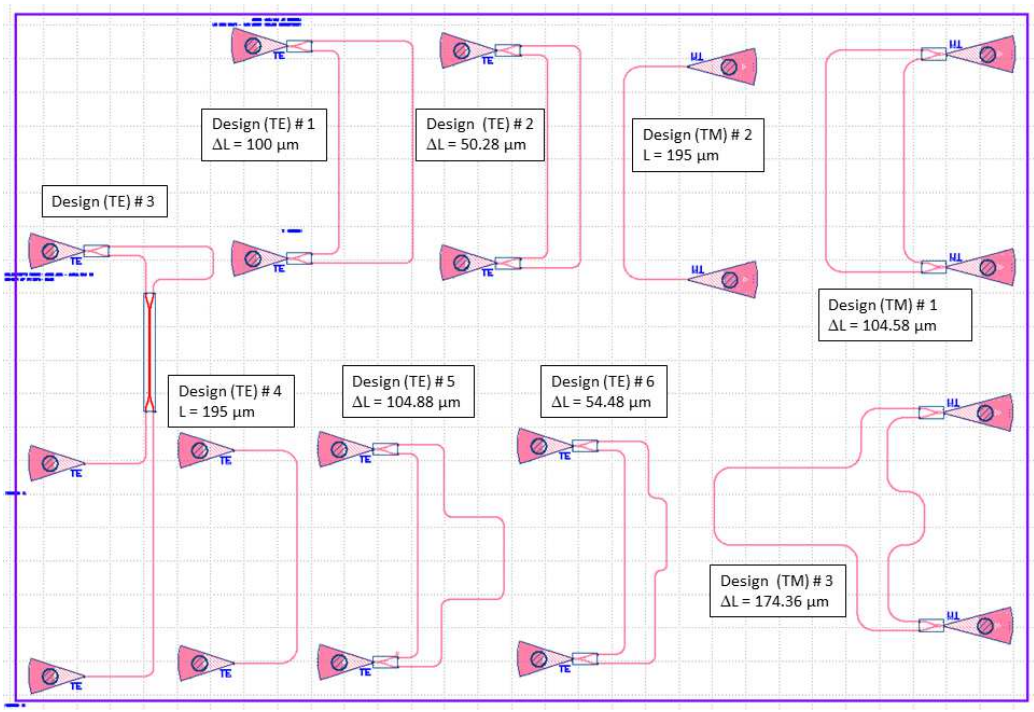

Fig. 6: gds layout used for fabrication

All waveguides are designed to have the same cross section (220 nm $\times$ 500 nm) but are varying in length. In particular, the dependence on the imbalance length (ΔL) is investigated. Table II gives an overview of the expected FSR for the TE-mode MZIs. The geometry (220 nm $\times$ 500 nm) was chosen because the S-parameter (Scattering Matrix) were provided in this class to be used in Lumerical INTERCONNECT simulations and also because this geometry allows for the WG to operate near the single-mode cut-off region.

Design Label	L_1 (μm)	L_2 (μm)	ΔL (μm)	FSR (nm)
TE #1	250	150	100	5.63
TE #2	200	149.72	50.28	16.28
TE #3	246.74	141.86	104.88	5.3
TE #4	204.47	150	54.48	10.49

TABLE II: WG length and FSR (at λ_0 = 1550 nm)

3.2. Simulation Results

3.2.1. Device level simulations using Lumerical MODE

In this class, Lumerical MODE [8] is used to simulate the waveguide structure and to extract the modes traveling in the WG along with the corresponding effective and group

index (n_{eff} and n_g). The simulated WG has a width of 0.5 μm and a height of 220 nm. The energy density of the first quasi-TE mode is given in figure 7a. It can be seen that most of the light is confined inside the WG, and almost no light leaks into the cladding oxide. A schematic of the strip wave guide is given in figure 7b. Since the Si-WG is surrounded by cladding oxide, it has a high optical confinement and lower cross-talk between other WGs, but it suffers from higher scattering loss due to sidewall roughness caused during manufacturing.

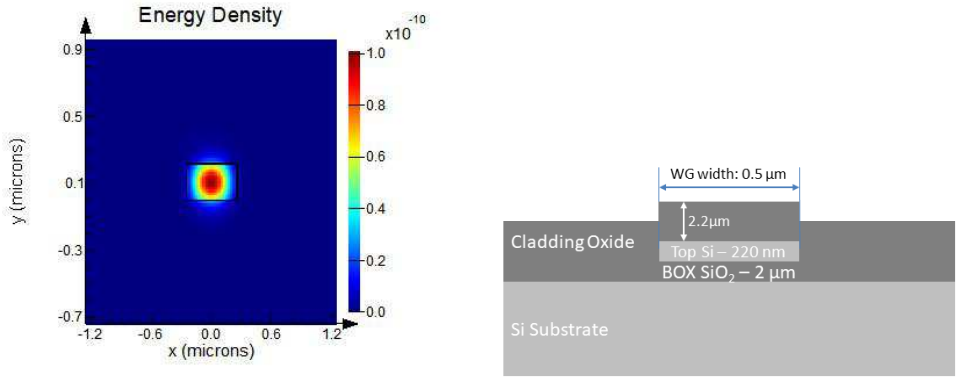

(a) Energy density of quasi-TE mode (b) Schematic cross-section of strip WG

Fig. 7: Energy density and schematic cross-section of strip wave guides

The effective index (n_{eff}) for this WG is shown in figure 8a, the group index is shown in figure 8b. At a wavelength of 1.55 μm, the effective index is 2.44 and the group index is 4.206; in general, the effective index decreases when the wavelength increases, whereas the group index increases when the wavelength increases. The main reason why n_{eff} decreases with an increasing wavelength is due to WG dispersion effects.

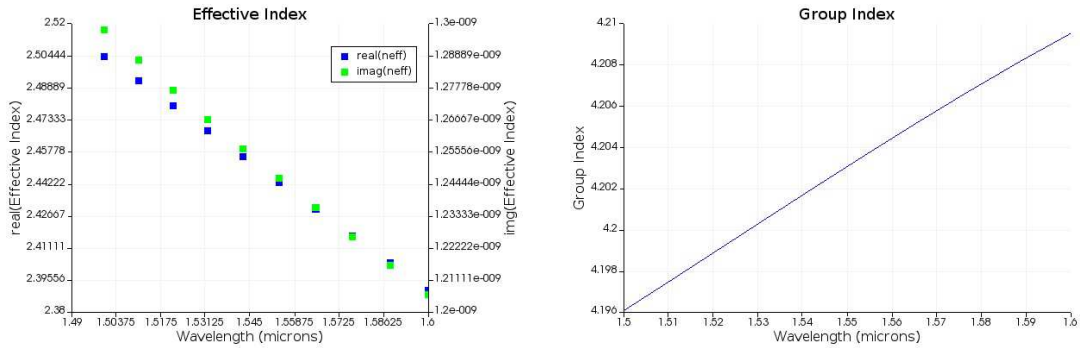

(a) Effective Index (b) Group Index

Fig. 8: Effective index and group index for a WG with a cross-section of 220 nm $\times$ 500 nm

The intensity of the electric field of the first four modes for a WG with a cross-section of 220 nm $\times$ 500 nm is given in figure 9. A mode is a solution to Maxwell's equations, taking into account the material parameters and the boundary conditions. It defines the way light

travels through space (or a medium). For a fixed geometry, the mode stays constant as it propagates down the WG. Depending on the geometry, the operating wavelength and the material properties, a WG can support single-mode or multi-mode operations.

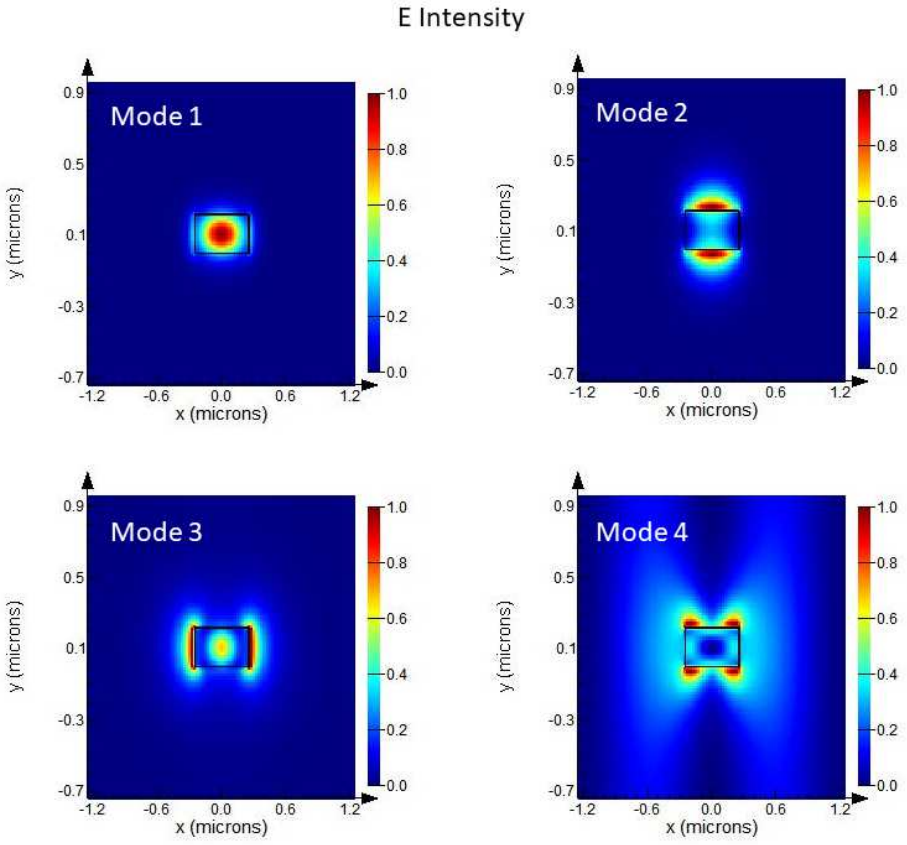

Fig. 9: Intensity of E-field for the first for modes

3.2.2. System level simulations using Lumerical INTERCONNECT

The MZI circuit for TE-polarized light (see figure 10) is simulated using the software Lumerical INTERCONNECT [8]. WG properties (i.e. n_{eff}, n_g, dispersion) are imported from Lumerical MODE simulations. Both WGs are modeled with the same geometry and material properties, but have different lengths.

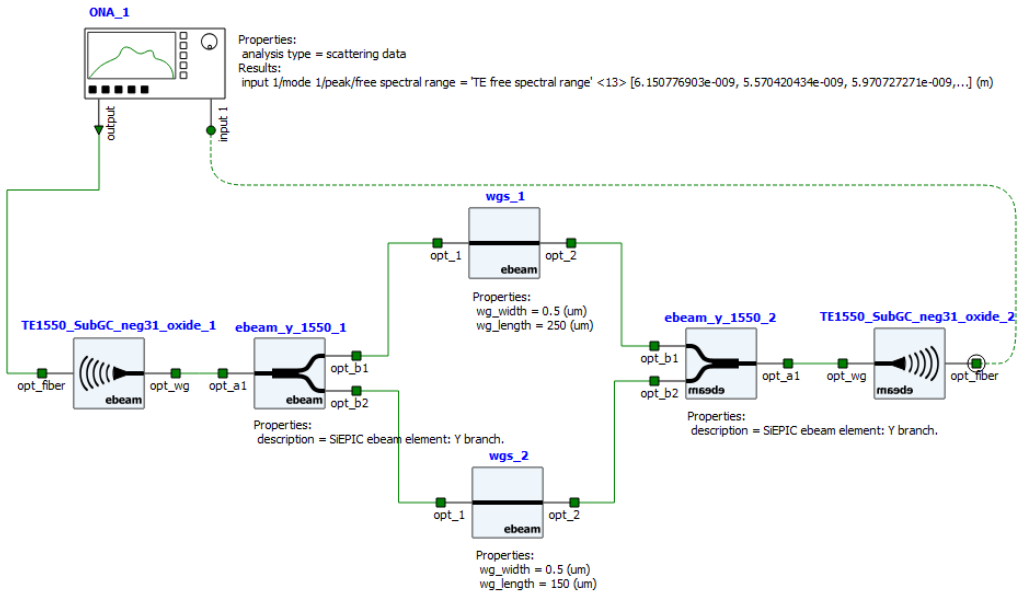

Fig. 10: MZI circuit simulation using Lumerical INTERCONNECT [8]

Figure 11 shows the FSR vs. wavelength for different imbalance lengths. It can be seen that the spread in FSR is smaller for a larger ΔL (i.e. 100 μm) whereas the spread in FSR increases when ΔL decreases (i.e. 50 μm).

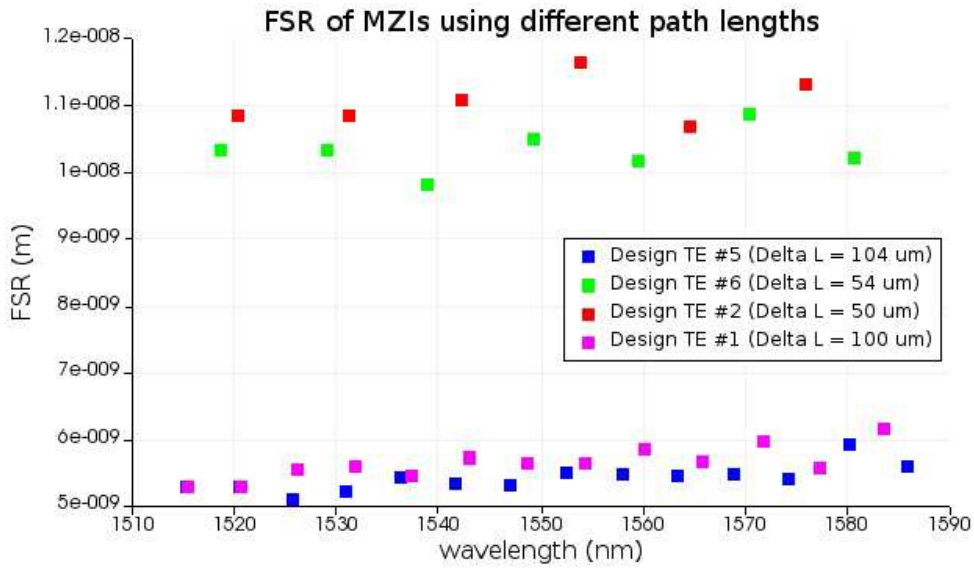

Fig. 11: FSR for MZIs with different imbalance length

Figure 12 shows the transmission spectrum of an imbalanced MZI using different lengths (ΔL).

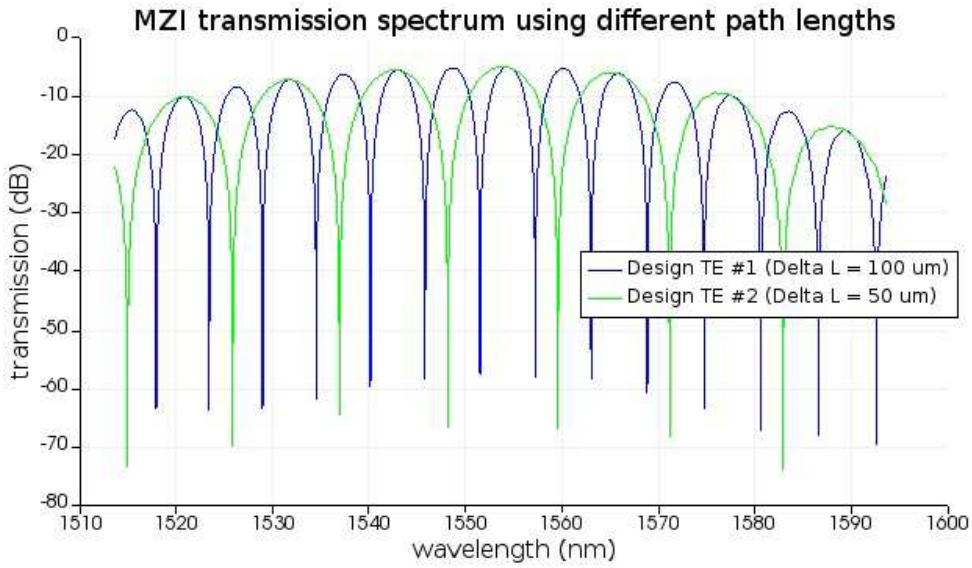

Fig. 12: Transmission for MZIs with different imbalance length

3.3. Manufacturing variability study - Corner Analysis

PIC often require that components are properly matched in terms of their center wavelength (typically 1.55 μm). However, in practice, it is often difficult to achieve the condition that the propagation constants (β_1 and β_2) of the WGs are well-matched due to variations in manufacturing. The dominant variations are the incoming top-Si thickness of the SOI substrate and the width of the fabricated WGs. These variations are present when comparing wafer-to-wafer and within-wafer data. The variation of the top-Si thickness can be gradual and also local (within a chip) which will result in optical component and circuit variations. Variation on feature size (i.e. width) strongly depend on the resist (i.e. variations in thickness and sensitivity, which can be age-related), exposure, development (i.e. time, age of chemicals) and etching (i.e. chamber conditions).

There are three main types of variations: systematic (occur all the time and can be accounted for, such as photo/etch bias), process drift (i.e. age of chemicals, chamber conditions) and random variations. In general, manufacturing variability can have a different effect depending on how the layout is drawn (i.e. how close the WGs are together). The corner-analysis method offers a quick way to analyze the ”worst cases” and takes typical process variations into account. The devices are fabricated on 6 inch, prime-grade wafers from Soitec, which have a mean top-Si thickness of 219.2 nm and a 6-sigma standard variation of 23.4 nm (or $\pm$ 3.9 nm, for one standard deviation). Based on experimental data and prior experience, the corner analysis is done for a range in top-Si thickness of 215.3 nm to 223.1 nm, and a width ranging from 470 nm to 510 nm ($\pm$ 30 nm), see figure 13.

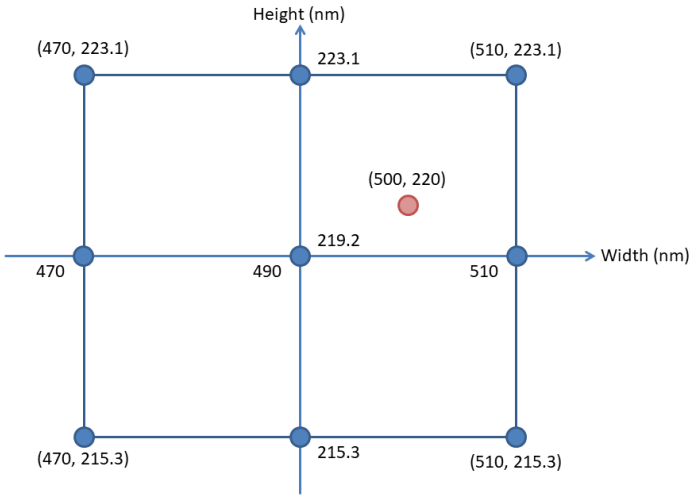

Fig. 13: Corner Analysis

The range in group index (n_g) based on this corner analysis is 4.129 to 4.208, and 5.67 to 5.78 for the range in FSR.

4. Fabrication

4.1. Applied Nanotools, Inc. NanoSOI process

The photonic devices were fabricated using the NanoSOI MPW fabrication process by Applied Nanotools Inc. [9] which is based on direct-write 100 keV electron beam lithography technology. Silicon-on-insulator wafers of 200 mm diameter, 220 nm device thickness and 2 μm buffer oxide thickness are used as the base material for the fabrication. The wafer was pre-diced into square substrates with dimensions of 25x25 mm, and lines were scribed into the substrate backsides to facilitate easy separation into smaller chips once fabrication was complete. After an initial wafer clean using piranha solution $(3:1$ $H_2SO_4 : H_2O_2)$ for 15 minutes and water/IPA rinse, hydrogen silsesquioxane (HSQ) resist was spin-coated onto the substrate and heated to evaporate the solvent. The photonic devices were patterned using a Raith EBPG 5000+ electron beam instrument using a raster step size of 5 nm. The exposure dosage of the design was corrected for proximity effects that result from the backscatter of electrons from exposure of nearby features. Shape writing order was optimized for efficient patterning and minimal beam drift. After the e-beam exposure and subsequent development with a tetramethylammonium sulfate (TMAH) solution, the devices were inspected optically for residues and/or defects. The chips were then mounted on a 4 handle wafer and underwent an anisotropic ICP-RIE etch process using chlorine after qualification of the etch rate. The resist was removed from the surface of the devices using a 10:1 buffer oxide wet etch, and the devices were inspected using a scanning electron microscope (SEM) to verify patterning and etch quality. A 2.2 μm oxide cladding was deposited using a plasma-enhanced chemical vapour deposition (PECVD) process based on tetraethyl orthosilicate (TEOS) at 300 $^{\circ}C$. Reflectrometry measurements were performed throughout the process to verify the device layer, buffer oxide and cladding thicknesses before delivery.

4.2. Measurement Setup

To characterize the devices, a custom-built automated test setup [10], [11] with automated control software written in Python was used [12]. An Agilent 81600B tunable laser was used as the input source and Agilent 81635A optical power sensors as the output detectors. The wavelength was swept from 1500 to 1600 nm in 10 pm steps. A polarization maintaining (PM) fibre was used to maintain the polarization state of the light, to couple the TE polarization into the grating couplers [13]. A 90° rotation was used to inject light into the TM grating couplers [13]. A polarization maintaining fibre array was used to couple light in/out of the chip [14].

4.3. Critical dimensions for fabricated structures

Metrology features were added (by the class instructor) in the design to establish a correlation between the CD size drawn in the gds (figure 14a) and the actual CD size after fabrication (figure 14b). The measured CD size for a 500 nm wide structure is between

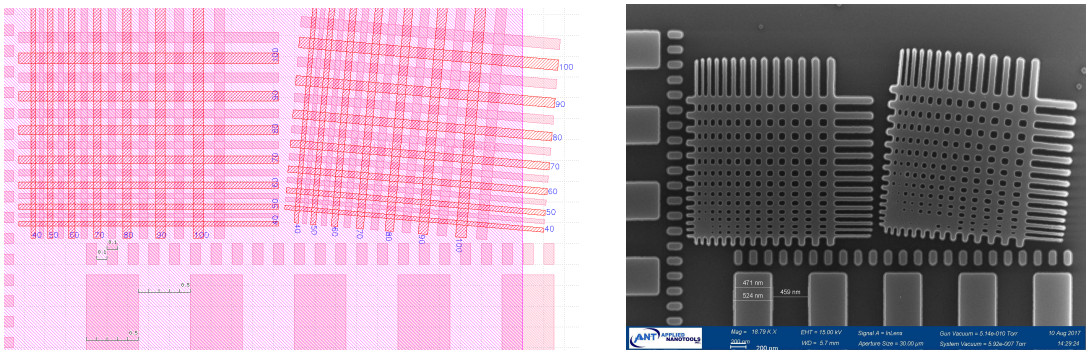

(a) CDs as drawn in the gds

(b) SEM picture of metrology area: CDs as fabricated

Fig. 14: Critical dimensions (CDs)

471 nm (bottom of the feature) and 524 nm (top of the feature), with an average of 497.5 nm ($= \frac{524-471}{2} + 471$). Using a height of 220 nm, the sidewall angle of the WGs can be estimated to 83°. The pitch size (between two 500 nm structures) was found to be 459 nm.

5. Experimental Data and Analysis

The experimental data is fitted using a matlab code provided in this class. The objective is to match the MZI experimental data with the matlab generated curve fit, which is useful to determine the WG parameters (group index, effective index, dispersion).
We start with the transfer function used to fit the MZI [5]:

$$F = 10 \cdot \log\left\{\frac{1}{4} \cdot \left|1 + \exp\left[-i \cdot \frac{2\pi \cdot n_{eff}(\lambda)}{\lambda} \cdot \Delta L - \alpha \cdot \frac{\Delta L}{2}\right]\right|^2\right\} + b \tag{16}$$

using $\lambda_0 = 1550$ nm. The propagation constant β can be expressed as [5]

$$\beta = \frac{2\pi \cdot n_{eff(\lambda)}}{\lambda} \tag{17}$$

α is the propagation loss and the constant b is used to shift the data up/down to match experimental results. If the measured data is calibrated correctly, the parameter b is the excess loss of the device.

The **effective index** (n_{eff}) can be approximated using a Taylor expansion [5]:

$$n_{eff} = n_1 + n_2 \cdot (\lambda - \lambda_0) + n_3 \cdot (\lambda - \lambda_0)^2 \tag{18}$$

using $\lambda_0 = 1550$ nm.
n_1 corresponds to the effective index (which is also the term responsible for a horizontal shift of the data).
n_2 is related to the group index using [5]

$$n_2 = \frac{n_g(\lambda) - n_1}{\lambda_0} \tag{19}$$

The **dispersion** is related to the slope of the group index vs. wavelength plot and gives an expression for n_3 [5]:

$$\frac{dn_g(\lambda)}{d\lambda} = -2 \cdot \lambda \cdot n_3 \tag{20}$$

The **group index** (n_g) can be extracted from the experimental data itself by plotting the transmission in dB vs. wavelength. The spacing of adjacent peaks is the **free-spectral range** (FSR) of that device [5]

$$\text{FSR} = \lambda_{n+1} - \lambda_n \tag{21}$$

Once the FSR is known, the group index can be extracted using [5]

$$\text{FSR} = \frac{\lambda^2}{n_g(\lambda) \cdot \Delta L} \tag{22}$$

The imbalance length ΔL is given in the design and may be different for each design.

5.1. Baseline correction

Any GC will limit the measurement bandwidth and will add insertion loss to the measurements. To remove this added insertion loss, a baseline correction is done on the experimental data. The data is fitted with a 4th order polynomial fit (see figure 15a) and then subtracted from the data. This procedure will result in a nearly flat transmission spectrum with its peaks close to 0 dB, as shown in figure (15b).

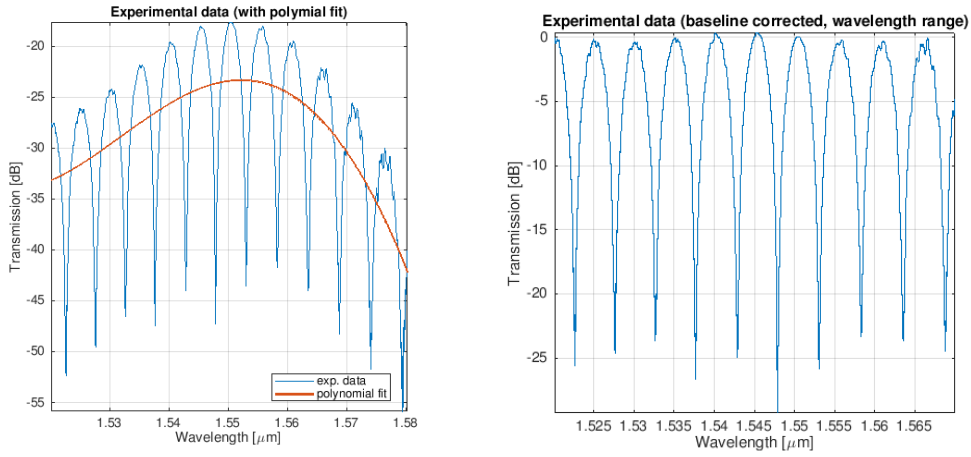

(a) Experimental data with polynomial fit

(b) Experimental data with baseline correction, resulting in a flat transmission spectrum

Fig. 15: Experimental Data with baseline correction

5.2. Loopback structures for calibration

The calibration is done using on-chip loopback structures. In theory, this should give feedback about the insertion loss, but may vary in practice due to manufacturing variability. Figure 16a shows the loopback structure designed to estimate the insertion loss caused by the two grating couplers; figure 16b shows the measured insertion loss, which is around 17 dB. In addition to the loss caused by grating couplers itself, there is also scattering loss in the waveguide which is associated with light scattering due to an unknown ammount of sidewall roughness.

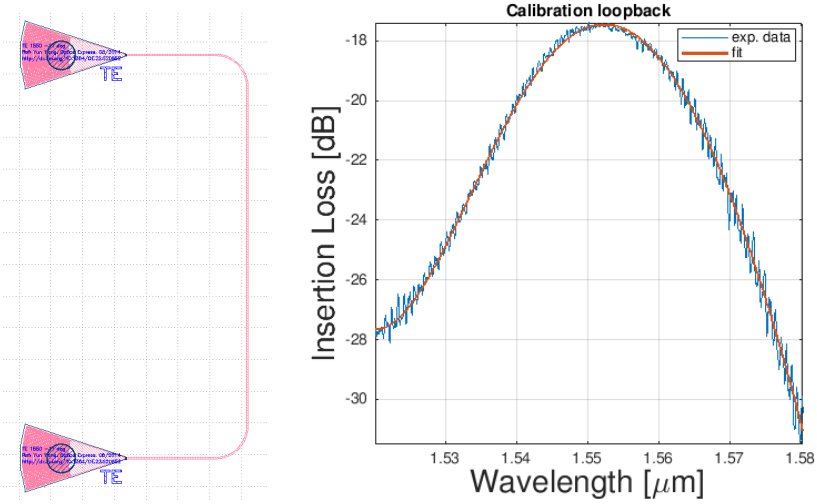

(a) Loopback structure as designed fro TE polarized light

(b) Measured data

Fig. 16: Loopback structure used for calibration of the insertion loss of the grating couplers

5.3. Fitting the MZI experimental data

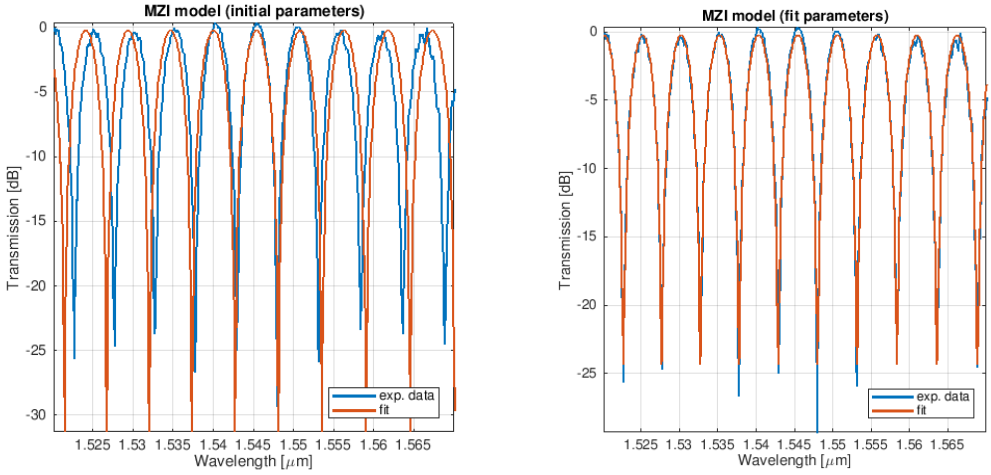

(a) MZI model using initial parameters (b) MZI model using fit parameters

Fig. 17: Fitting the MZI experimental data

The FSR can be estimated from the spacing between the peaks in the transmission spectrum (see figure 17), and is found to be 5.158 nm.
The group index is 4.1562 for $\lambda_0 = 1550$ nm, and is plotted in the wavelength range of interest in figure 18. Both values are well in agreement with what was obtained by the corner analysis (see page 13) for a waveguide with a cross-section of 500 nm $\times$ 200 nm.

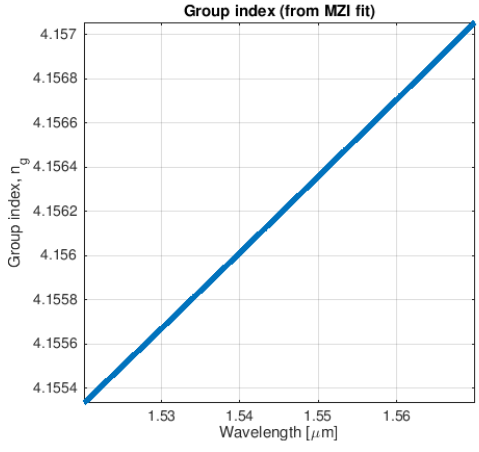

Fig. 18: Group index for measured MZI structure with $\Delta L = 100\mu m$

6. Summary

In this class project, MZIs were fabricated using SOI substrates with a top Si thickness of 200 nm. The waveguide width was kept constant at 500 nm, and the imbalance length was varied. The experimental data for the chosen device (Design (TE) #1) with an imbalance length of 100 μm was analyzed and is in good agreement with the expected result obtained from simulations.

7. Acknowledgments

I acknowledge the edX UBCx Phot1x Silicon Photonics Design, Fabrication and Data Analysis course, which is supported by the Natural Sciences and Engineering Research Council of Canada (NSERC) Silicon Electronic-Photonic Integrated Circuits (SiEPIC) Program. The devices were fabricated by Richard Bojko at the University of Washington Washington Nanofabrication Facility, part of the National Science Foundations National Nanotechnology Infrastructure Network (NNIN), and Cameron Horvath at Applied Nanotools, Inc. Enxiao Luan performed the measurements at The University of British Columbia. We acknowledge Lumerical Solutions, Inc., Mathworks, Mentor Graphics, Python, and KLayout for the design software.

References

[1] BRECK HITZ, ”Tiny Mach-Zehnder Modulator Operates at 10 Gb/s”, published in https://www.photonics.com/Article.aspx?AID=32251
[2] Lukas Chrostowski, Michael Hochberg, page 111 in ”Silicon Photonics Design: From Devices to Systems”, Cambridge University Press, 2015
[3] Screenshot from gds used in this class; the PDK library can be found here: https://github.com/lukasc-ubc/SiEPIC_EBeam_PDK/wiki/Component-Library-description
[4] https://www.rp-photonics.com/propagation_constant.html
[5] Lecture notes from EdX class ”Silicon Photonics Design, Fabrication and Data Analysis”
[6] https://www.rp-photonics.com/effective_refractive_index.html
[7] Lukas Chrostowski, Michael Hochberg, page 114 in ”Silicon Photonics Design: From Devices to Systems”, Cambridge University Press, 2015
[8] https://www.lumerical.com/tcad-products/
[9] http://www.appliednt.com/nanosoi;Edmonton,Canada
[10] Lukas Chrostowski, Michael Hochberg, chapter 12 in ”Silicon Photonics Design: From Devices to Systems”, Cambridge University Press, 2015
[11] http://mapleleafphotonics.com, Maple Leaf Photonics, Seattle WA, USA.
[12] http://siepic.ubc.ca/probestation, using Python code developed by Michael Caverley.
[13] Yun Wang, Xu Wang, Jonas Flueckiger, Han Yun, Wei Shi, Richard Bojko, Nicolas A. F. Jaeger, Lukas Chrostowski, ”Focusing sub-wavelength grating couplers with low back reflections for rapid prototyping of silicon photonic circuits”, Optics Express Vol. 22, Issue 17, pp. 20652-20662 (2014) doi: 10.1364/OE.22.020652
[14] www.plcconnections.com, PLC Connections, Columbus OH, USA.